Biomaterials 34 (2013) 6785–6796

Contents lists available at SciVerse ScienceDirect

Biomaterials

journal homepage: www.elsevier.com/locate/biomaterials

Transdermal regulation of vascular network bioengineering using a photopolymerizable methacrylated gelatin hydrogel

Ruei-Zeng Lin [a], Ying-Chieh Chen [b,c], Rafael Moreno-Luna [a], Ali Khademhosseini [c,d,e], Juan M. Melero-Martin [a,*]

[a] Department of Cardiac Surgery, Boston Children's Hospital, Harvard Medical School, Boston, MA 02115, USA
[b] Department of Applied Science, National Hsinchu University of Education, Taiwan
[c] Department of Medicine, Center for Biomedical Engineering, Brigham and Women's Hospital, Harvard Medical School, Boston, MA 02115, USA
[d] Harvard-MIT Division of Health Sciences and Technology, Massachusetts Institute of Technology, Cambridge, MA 02139, USA
[e] Wyss Institute for Biologically Inspired Engineering, Harvard Medical School, Boston, MA 02155, USA

ARTICLE INFO

Article history:
Received 11 April 2013
Accepted 24 May 2013
Available online 14 June 2013

Keywords:
Endothelial colony-forming cells
Endothelial progenitor cells
GelMA
Hydrogel
Vascular network

ABSTRACT

The search for hydrogel materials compatible with vascular morphogenesis is an active area of investigation in tissue engineering. One candidate material is methacrylated gelatin (GelMA), a UV-photocrosslinkable hydrogel that is synthesized by adding methacrylate groups to the amine-containing side-groups of gelatin. GelMA hydrogels containing human endothelial colony-forming cells (ECFCs) and mesenchymal stem cells (MSCs) can be photopolymerized ex vivo and then surgically transplanted in vivo as a means to generate vascular networks. However, the full clinical potential of GelMA will be best captured by enabling minimally invasive implantation and in situ polymerization. In this study, we demonstrated the feasibility of bioengineering human vascular networks inside GelMA constructs that were first subcutaneously injected into immunodeficient mice while in liquid form, and then rapidly crosslinked via transdermal exposure to UV light. These bioengineered vascular networks developed within 7 days, formed functional anastomoses with the host vasculature, and were uniformly distributed throughout the constructs. Most notably, we demonstrated that the vascularization process can be directly modulated by adjusting the initial exposure time to UV light (15–45 s range), with constructs displaying progressively less vascular density and smaller average lumen size as the degree of GelMA crosslinking was increased. Our studies support the use of GelMA in its injectable form, followed by in situ transdermal photopolymerization, as a preferable means to deliver cells in applications that require the formation of vascular networks in vivo.

1. Introduction

The discovery of highly proliferative endothelial colony-forming cells (ECFCs) in human peripheral blood [1,2] and in the vessel wall of some blood vessels [3] has created a promising opportunity to obtain large quantities of readily available endothelial cells (ECs) for autologous vascular therapies. Indeed, multiple studies have shown that ECFCs have a robust vasculogenic potential that can be exploited to generate long-lasting, stable vascular networks in vivo [4–7]. A critical requirement for bioengineering vascular networks is the use of a suitable biomaterial that can serve as a scaffold for the cells. Over the last few years, a variety of natural hydrogel biomaterials have been shown to be compatible with ECFC-mediated vascular morphogenesis, including Matrigel [4,8], type-I collagen [5,9,10], and fibrin gels [7,11], which indicates the versatility of ECFCs with regards to natural hydrogels in vivo. However, the properties of these materials are not always ideal for tissue engineering applications. For instance, Matrigel is not suitable for clinical use because it is derived from murine tumors [12]. Fibrin hydrogels have limitations such as poor mechanical stability or suboptimal durability [13]. Collagen hydrogels also have limitations in terms of extensive contraction, poor mechanical properties, and rapid degradation [14], all of which provide challenges towards their utilization as permanent graft material. Moreover, full polymerization of most collagen formulations at body temperature does not occur immediately, which may compromise gel-cell confinement if implanted in highly mobile tissues such as skeletal muscles or myocardium.

* Corresponding author. Department of Cardiac Surgery, Boston Children's Hospital, 300 Longwood Ave., Enders 349, Boston, MA 02115, USA. Tel.: +1 617 919 3072; fax: +1 617 730 0235.
E-mail address: juan.meleromartin@childrens.harvard.edu (J.M. Melero-Martin).

0142-9612/$ – see front matter © 2013 Elsevier Ltd. All rights reserved.
http://dx.doi.org/10.1016/j.biomaterials.2013.05.060

In response to these limitations, the search for improving the properties of naturally occurring extracellular matrix (ECM) proteins has become a priority in tissue engineering research [15]. This can be achieved by chemical functionalization of ECM proteins, an approach that was initially proposed to improve the usability of biomaterials [16]. A recent example of material functionalization is the development of photocrosslinkable methacrylated gelatin (GelMA) hydrogels, which are synthesized by adding methacrylate groups to the amine-containing side-groups of gelatin [17]. Recently, we demonstrated that this material is fully compatible with ECFC-based vascular morphogenesis [18], and thus we proposed its use for vascular bioengineering applications. In addition, we demonstrated that our GelMA formulation can polymerize very rapidly (~15 s upon exposure to UV light in the presence of a photoinitiator) and proposed that this rapid polymerization would be a critical feature to avoid hydrogel dissemination at the implantation site.

Photocrosslinking of GelMA has been demonstrated ex vivo [17–20], but in situ polymerization following its injection in vivo remains untested. For example, our previous pre-clinical study on vascular network formation was conducted with cell-laden GelMA constructs that were first polymerized ex vivo and then surgically implanted into the subcutaneous space of immunodeficient mice [18]. However, enabling hydrogel injection and in situ polymerization would be more desirable because (i) it would eliminate the need for surgical incisions, (ii) enable the cell-laden hydrogel solution to acquire complex shapes and precise dimensions in situ, prior to polymerization, and (iii) improve intimate contact of the polymer with the surface micro-roughness of the tissue at the implantation site [21]. Here, we addressed whether GelMA hydrogel can be transdermally photocrosslinked and how this procedure affects capillary morphogenesis in the context of vascular network bioengineering. We have carried out preclinical studies with immunodeficient mice and demonstrated that functional human vascular networks can be generated in situ by means of transdermal photopolymerization, an approach that enables tuning the final vascular density inside the GelMA hydrogel constructs.

2. Material and methods

2.1. Synthesis of GelMA

GelMA was synthesized as previously described [18]. Briefly, type A porcine skin gelatin (Sigma–Aldrich, St. Louis, MO) was dissolved in Dulbecco's phosphate buffered saline (DPBS; Invitrogen, Carlsbad, CA) at 60 °C to make a 10% (w/v) gelatin solution. Methacrylic anhydride (Sigma–Aldrich) was added to the gelatin solution at a rate of 0.5 mL/min under stirring conditions to a final concentration of 1% (v/v). The mixture was allowed to react for 3 h at 50 °C. After a 5× dilution with additional warm DPBS, the GelMA solution was dialyzed against deionized water using 12–14 kDa cutoff dialysis tubes (Spectrum Laboratories, Rancho Dominguez, CA) for 7 days at 40 °C to remove unreacted methacrylic anhydride and additional by-products. The dialyzed GelMA solutions were lyophilized and stored at −80 °C.

2.2. UV light source and intensity

OmniCure S2000 UV lamp (Lumen Dynamics, Ontario, Canada) was used to provide UV exposure in this study. UV intensity was adjusted using a UV intensity meter (G&R Labs, Santa Clara, CA). Transdermal photocrosslinking was achieved with UV intensity of 40 mW/cm^2, which corresponded to 7.5 mW/cm^2 transdermally (nude mice skin). Direct (non-transdermal) photocrosslinking was achieved with UV intensity of 7.5 mW/cm^2.

2.3. Transdermal photocrosslinking of GelMA hydrogels

A GelMA prepolymer solution was prepared by dissolving the freeze-dried GelMA (5 w/v% final) and the photoinitiator (Irgacure 2959, 0.5 w/v%; CIBA Chemicals, Basel, Switzerland) in DPBS at 80 °C and allowed to cool down to 37 °C in a water bath. For a better visualization in specific cases, trypan blue dye (5% v/v) was added to the GelMA prepolymer solution. 200 μL of GelMA solution was injected using a 26G needle into the subcutaneous space of nu/nu mice and polymerization was achieved by transdermal exposure to UV light.

2.4. Transmission spectrum of murine nu/nu skin

The optical transmission of nu/nu mouse skin was measured using a UV–visible/NIR spectrophotometer (U-4100; Hitachi High-Technologies Corporation, Japan) over the range of 200–2600 nm. Skin slices were carefully removed (2 × 2 cm^2 area) from the backs of 6-week-old nu/nu mice, attached to a quartz slide, and the absolute transmission spectrum was measured.

2.5. Mechanical characterization of GelMA hydrogels

Rheological measurements at oscillatory shear deformation were carried out with a AR-G2 rheometer (TA Instruments) using parallel rough plates of 25 mm diameter and plate-to-plate distance of 1 mm. GelMA hydrogels (25 mm in diameter and 1 mm in height) were placed positioned on the temperature-controlled plate and the mechanical spectra were recorded in a constant strain mode with a low deformation of 0.01 maintained over the frequency range of 0.01–100 Hz (rad/s) at 37 °C [22].

2.6. Degradability assay

Enzymatic degradation of GelMA hydrogels was carried out in DPBS containing 2 μg/mL collagenase A (Roche Diagnostics, Indianapolis, IN) at 37 °C. The percentage of hydrogel mass loss was determined after 4 h as previously described [18].

2.7. TUNEL assay

The skin of nude mice was exposed to UV light (40 mW/cm^2) for either 15, 30, 45, 90, or 300 s. The exposed skin was harvested 2 days later from the euthanized mice, fixed in 10% buffered formalin overnight, embedded in paraffin, and sectioned (7-μm-thick). The presence of apoptotic cells was analyzed by Terminal deoxynucleotidyl transferase dUTP nick end labeling (TUNEL) staining using a TdT In Situ Apoptosis Detection Kit (R&D System, Minneapolis, MN). Cell nuclei were counterstained with DAPI. Percentage of apoptotic nuclei (TUNEL$^+$/DAPI$^+$) was examined under a fluorescent microscope and counted using ImageJ software (NIH). False positive signals caused by erythrocytes were carefully ruled out by the lack of nuclei.

2.8. Cell culture

ECFCs and MSCs were isolated from human umbilical cord blood and bone marrow, respectively, as previously described [4]. ECFCs were cultured on 1% gelatin-coated plates using ECFC-medium: EGM-2 (except for hydrocortisone; Lonza, Walkersville, MD) supplemented with 20% FBS (Hyclone, Logan, UT), 1× glutamine-penicillin-streptomycin (GPS; Invitrogen). MSCs were cultured on uncoated plates using mesenchymal stem cell growth medium (MSCGM; Lonza) with 10% FBS, 1× GPS and 10 ng/mL bFGF (R&D System). ECFCs and MSCs between passages 6 and 9 were used for all the experiments. DsRed-expressing ECFCs were generated as previously described [18].

2.9. Cell viability assay

Cell-laden GelMA hydrogels were digested with 1 mg/mL collagenase-A solution for 30 min at 37 °C. Retrieved cells were labeled with LIVE/DEAD® Cell Viability reagents (Invitrogen) and the number of viable cells counted under a fluorescent microscope.

2.10. Cell attachment assay

Viable cells (5 × 10^4) were seeded in triplicates onto 1% gelatin-coated 24-well plates using ECFC- or MSC-medium. Unattached cells were removed after 3 h by thoroughly washing each well with fresh medium. Attached cell nuclei were stained with DAPI and counted under a fluorescent microscope.

2.11. Proliferation assay

Cells were seeded in triplicates onto 1% gelatin-coated 24-well plates (5 × 10^3 viable cell/cm^2) using ECFC- or MSC-medium. Plating efficiency was determined at 24 h. Cells were then treated for 48 h using fresh medium. Cells were trypsinized and counted using a hemocytometer. Values were normalized to cell numbers at 24 h.

2.12. Cell spreading assay

GelMA solution containing either ECFCs or MSCs (1 × 10^6/mL) was exposed to UV light (7.5 mW/cm^2) for 15, 30, or 45 s. Polymerized cell-laden GelMA constructs were cultured in vitro for 2 days, and were then fixed for 30 min in 3.2% paraformaldehyde, permeabilized with 0.5% Triton X-100, and stained with FITC-phalloidin (Invitrogen) and DAPI. Cells were imaged under a fluorescent microscope and the area occupied by each cell was measured using ImageJ software.

2.13. Transmigration assay

Transwell inserts (6.5 mm diameter, 8.0 μm pore size; Corning Incorporated, Corning, NY) were coated with 20 μL GelMA solution and then exposed to UV light for 15, 30, or 45 s. ECFCs or MSCs (1×10^4 cells in 100 μL of EBM-2, 5% FBS) were added to the top compartment of the transwell inserts. Inserts were then transferred into 24-well plates containing 1 mL/well of EC-medium. After 24 h, transmigrated cells were visualized on the bottom side of the insert membrane, stained with DAPI, and counted under a fluorescent microscope.

2.14. Implantation of GelMA constructs into mice

A GelMA prepolymer solution was prepared by dissolving GelMA (5 w/v% final) and Irgacure 2959 (0.5 w/v%) in DPBS at 80 °C and then cooled to 37 °C in a water bath. ECFCs and MSCs (2×10^6 total; 40:60 ECFCs/MSCs ratio) were resuspended in 200 μL of GelMA solution and the mixture was polymerized either ex-vivo or in-vivo and implanted as follows: (1) ex-vivo-UV group - the cell/GelMA mixture was polymerized by exposure to 7.5 mW/cm^2 UV light for 15 s at 37 °C. Subsequently, polymerized cell-laden constructs were washed in PBS twice and subcutaneously implanted into 6-week-old male athymic nu/nu mice ($n = 4$). (2) in-vivo-UV - the cell/GelMA mixture was injected using a 26G needle into the subcutaneous space of nu/nu mice and polymerization was achieved by transdermal exposure to UV light for indicated exposure time. All animal experiments were conducted under a protocol approved by the Institutional Animal Care and Use Committee at Boston Children's Hospital. Matrigel (BD Biosciences, San Jose, CA) and bovine type-I collagen (Trevigen, Gaithersburg, MD) hydrogels served as controls and were used as previously described [10,23].

2.15. Histology and immunohistochemistry

Implants were removed from euthanized mice, fixed in 10% buffered formalin overnight, embedded in paraffin, and sectioned (7-μm-thick). Hematoxylin and eosin (H&E)-stained sections were examined for the presence of blood vessels containing red blood cells. For immunohistochemistry, sections were deparaffinized and antigen retrieval was carried out by heating the sections in Tris–EDTA buffer (10 mM Tris-Base, 2 mM EDTA, 0.05% Tween-20, pH 9.0). The sections were blocked for 30 min in 5% blocking serum and incubated with primary antibodies for 1 h at room temperature. The following primary antibodies were used: mouse anti-human CD31 (1:50; Clone JC70A; DakoCytomation, Carpinteria, CA), mouse anti-α-SMA (1:200; Clone 1A4; Sigma–Aldrich), and mouse IgG (1:50; DakoCytomation). Horseradish peroxidase (HRP)-conjugated mouse secondary antibody (1:200; Vector Laboratories, Burlingame, CA) and 3,3′-diaminobenzidine (DAB) were used for detection of hCD31, followed by hematoxylin counterstaining and Permount mounting. Fluorescent staining was performed using rhodamine-conjugated UEA-1 (20 μg/mL) and FITC-conjugated secondary antibodies (1:200; Vector Laboratories) followed by DAPI counterstaining.

2.16. Microvessel density

Microvessel density was reported as the average number of erythrocyte-filled vessels (vessels/mm^2) in sections from the middle of the implants as previously described [8]. The entire area of each section was analyzed. Values reported for each experimental condition correspond to mean ± S.D. obtained from four individual mice. Vessel lumen sizes were determined by measuring thirty representative hCD31$^+$ vessels using ImageJ software. Sections were stained with DAPI and cellularity was reported as the average number of nuclei per unit of area (cells/mm^2).

2.17. Quantification of host cell infiltration

Implants and the surrounding host tissues were harvested at day 2 from euthanized mice and enzymatically (collagenase and dispase) digested for 1 h at 37 °C. The retrieved cells were incubated with PerCP-conjugated anti-mouse CD45 (1:100; BD Biosciences), PE-conjugated anti-mouse CD11b (1:100; BD Biosciences), FITC-conjugated mLy6G (1:50; eBiosciences), PE-conjugated anti-mouse CD29 (1:100; eBiosciences), and APC-conjugated anti-mouse CD31 (1:50; eBiosciences) antibodies. Murine myeloid cells were identified as mCD45$^+$/mCD11b$^+$ cells. Murine ECs were identified as mCD45$^-$/mCD29$^+$/mCD31$^+$ cells. Flow cytometric analyses were performed using a Guava easyCyte 6HT/2L flow cytometer (Millipore Corporation, Billerica, MA) and FlowJo software (Tree Star Inc., Ashland, OR).

2.18. Microscopy

All images were taken with an Axio Observer Z1 inverted microscope (Carl Zeiss, Berlin, Germany) using AxioVision Rel. 4.8 software. Phase microscopy images were taken with an AxioCam MRm camera and 5×/0.16 or 10×/0.3 objective lens. All fluorescent images were taken with an ApoTome.2 Optical sectioning system (Carl Zeiss) and 20×/0.8 or 40×/1.4 oil objective lens. Non-fluorescent images were taken with an AxioCam MRc5 camera using a 40×/1.4 objective oil lens.

2.19. Statistical analysis

Data were expressed as mean ± S.D. and means were compared using unpaired Student's *t* tests. Comparisons between multiple groups were performed by ANOVA followed by Bonferroni's post-test analysis. All statistical analyses were performed using GraphPad Prism version 5 software. $P < 0.05$ was considered statistically significant.

3. Results

3.1. In vitro polymerization of GelMA

Transdermal polymerization of GelMA was evaluated in vitro using skin from euthanized mice (Fig. 1). We first demonstrated that light can be transmitted (~15–40% transmission) through the skin of nude mice using our OmniCure S2000 UV lamp (320–500 nm) (Fig. 1A) and that GelMA polymerization was achieved after just 15 s of transdermal exposure to UV light (Fig. 1B). Moreover, we were able to modify the degree of transdermal polymerization by varying the exposure time to UV light (Fig. 1C, D). We tested exposure times ranging from 0 to 300 s. As expected, longer exposures to UV light yielded higher degree of polymerization, as evidenced by the hydrogel mechanical properties (both elastic and viscous modulus; Fig. 1C and Supplementary Fig. 1) and the resistance to enzymatic degradation (Fig. 1D). The wavelength generated by our UV lamp varies between 320 and 500 nm (Fig. 1A). This spectrum includes blue and violet visible light (380–500 nm) and UVA light (315–400 nm), but not UVB (280–315 nm) or UVC (100–280 nm) light (UVB and UVC light are deemed as more damaging to the skin [24]). Nevertheless, we looked for the presence of apoptotic cells in the skin of nude mice 48 h after they were exposed to UV light (Fig. 1E, F). We found that the skin of mice that were exposed for 15–90 s had a similar number of apoptotic cells as compared to the skin of unexposed mice (1.4%–1.9% TUNEL$^+$ cells). Only when the exposure time was significantly increased (300 s), did we observe a significant increase in the number of apoptotic cells (3.3% TUNEL$^+$ cells). Therefore, our working range of UV light exposure (15–45 s) was deemed as sufficiently safe.

3.2. In vivo transdermal GelMA polymerization and vasculogenesis

We compared transdermal photocrosslinking of cell-laden GelMA following subcutaneous injection into nude mice (referred to as in-vivo-UV group; UV light applied for 15 s; Fig. 2B) with the results of GelMA constructs that were polymerized ex vivo prior to surgical implantation (ex-vivo-UV; also UV applied for 15 s; light intensity was adjusted to achieve the same degree of photopolymerization; Fig. 2A). First, we confirmed that neither of these approaches had a negative effect on cell viability (>89% viable cells in both groups), as assessed by tests performed on cells retrieved from both sets of constructs after 3 h in vivo (Fig. 2C). Moreover, we found that explanted constructs that were cultured ex vivo for 3 additional days (after the initial 3 h in vivo) developed extensive ECFC-lined capillary-like networks (Fig. 2D), indicating that the initial administration of UV light ex vivo or in vivo (transdermally) had no negative impact on cell functionality.

To assess the formation of vascular networks in vivo after transdermal photocrosslinking we injected cell-laden GelMA (200 μL of hydrogel seeded with 8×10^5 ECFCs and 1.2×10^6 MSCs) into nude mice and applied UV light for 15 s at the implantation site (Fig. 2E). Ex-vivo-UV GelMA hydrogels served as a control. After 7 days, the constructs were explanted and examined for the presence of vascular structures. Histological examination carried out by H&E staining revealed that the extent of vascular network formation was different between the ex-vivo-UV and the in-vivo-UV GelMA constructs (Fig. 2F, G). In the in-vivo-UV group, numerous blood vessels

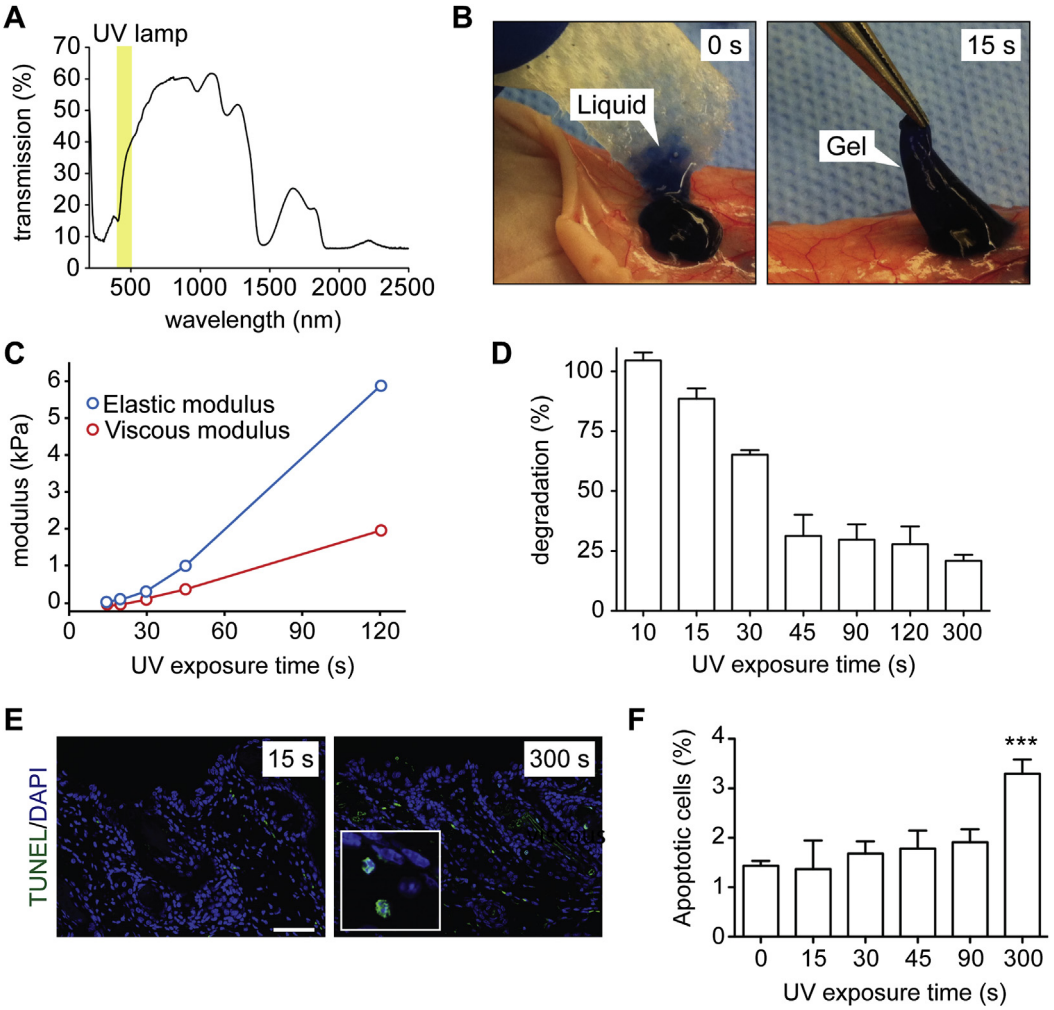

Fig. 1. Photopolymerization of GelMA. (A) Transmission spectrum of murine nu/nu skin. The yellow band corresponds to the wavelength range of our OmniCure S2000 UV lamp (320–500 nm). (B) Transdermal polymerization of GelMA after 15 s exposure to UV light (right panel). GelMA remained a liquid in the absence of UV light (0 s; left panel). Trypan blue was added to facilitate visualization. (C) Mechanical properties (elastic and viscous modulus) of GelMA constructs after transdermal photopolymerization using different UV exposure times. (D) Degradation profiles upon 4 h incubation with collagenase. (E) Nude mice were exposed to UV light. Two days later, the dermis under the exposed skin was examined to determine the presence of apoptotic (TUNEL$^+$) cells (scale bars 50 μm). Cell nuclei were stained with DAPI. High magnification of TUNEL$^+$ cells is depicted in the inset. (F) Percentage of apoptotic cells in the dermis of mice that were subjected to different UV exposure times. The data are presented as the mean ± SD. ***$p < 0.001$. (For interpretation of the references to color in this figure legend, the reader is referred to the web version of this article.)

containing erythrocytes were uniformly distributed throughout the explants (Fig. 2F). In contrast, there were fewer perfused blood vessels in the ex-vivo-UV GelMA explants (67.26 ± 12.16 lumens/mm^2 in the ex-vivo-UV vs. 374.7 ± 87.09 lumens/mm^2 in the in-vivo-UV; Fig. 2G). Further examination of explants from the in-vivo-UV group revealed that the microvessels stained positively for human CD31 (Fig. 2H) and UEA-1 (Fig. 2I), confirming that the lumens were lined with the implanted human ECFCs. Additionally, human microvessels were predominantly covered by α-SMA$^+$ perivascular cells (Fig. 2I), indicating the formation of stable vascular structures.

To explain the difference in microvascular density between the ex-vivo-UV and the in-vivo-UV groups, we carried out extensive histological examination of the explants at day 7 (Fig. 3 and Supplementary Fig. 2). The main difference was found in the degree of intimate contact (defined as lack of visible gaps) between the boundary of the GelMA construct (referred to as G in Fig. 3) and the surrounding mouse tissue (M), with in-vivo-UV constructs showing a better integration than the ex-vivo-UV ones (Fig. 3A, B). We quantified the percentage of construct boundary that had full integration with murine tissue and found that the difference between in-vivo-UV constructs (91 ± 6% integration) and ex-vivo-UV constructs (52 ± 7%) was statistically significant (Fig. 3C).

The degree of integration with host tissue was found intimately related to regional differences in vascular uniformity and density inside the constructs (Fig. 3D, E and Supplementary Fig. 2). Specifically, those regions with full G-M integration had higher number of perfused blood vessels than regions with boundary gaps (G-gap), which explains the lower overall microvessel density in the ex-vivo-UV constructs that contained more G-gap contours (Fig. 2G). Histological quantification revealed that those regional differences were closely associated with differences in cellularity (Fig. 3F), total vascularity (Fig. 3G), and human (ECFC-lined) vascularity (Fig. 3H and Supplementary Fig. 2), with higher presence of both cells and blood vessels in the well-integrated G-M regions. In fact, when we accounted for only well-integrated G-M regions, there were no differences in cellularity and vascularity between in-vivo-UV and ex-vivo-UV explants, indicating that intimate contact between construct and host tissue was indeed critical.

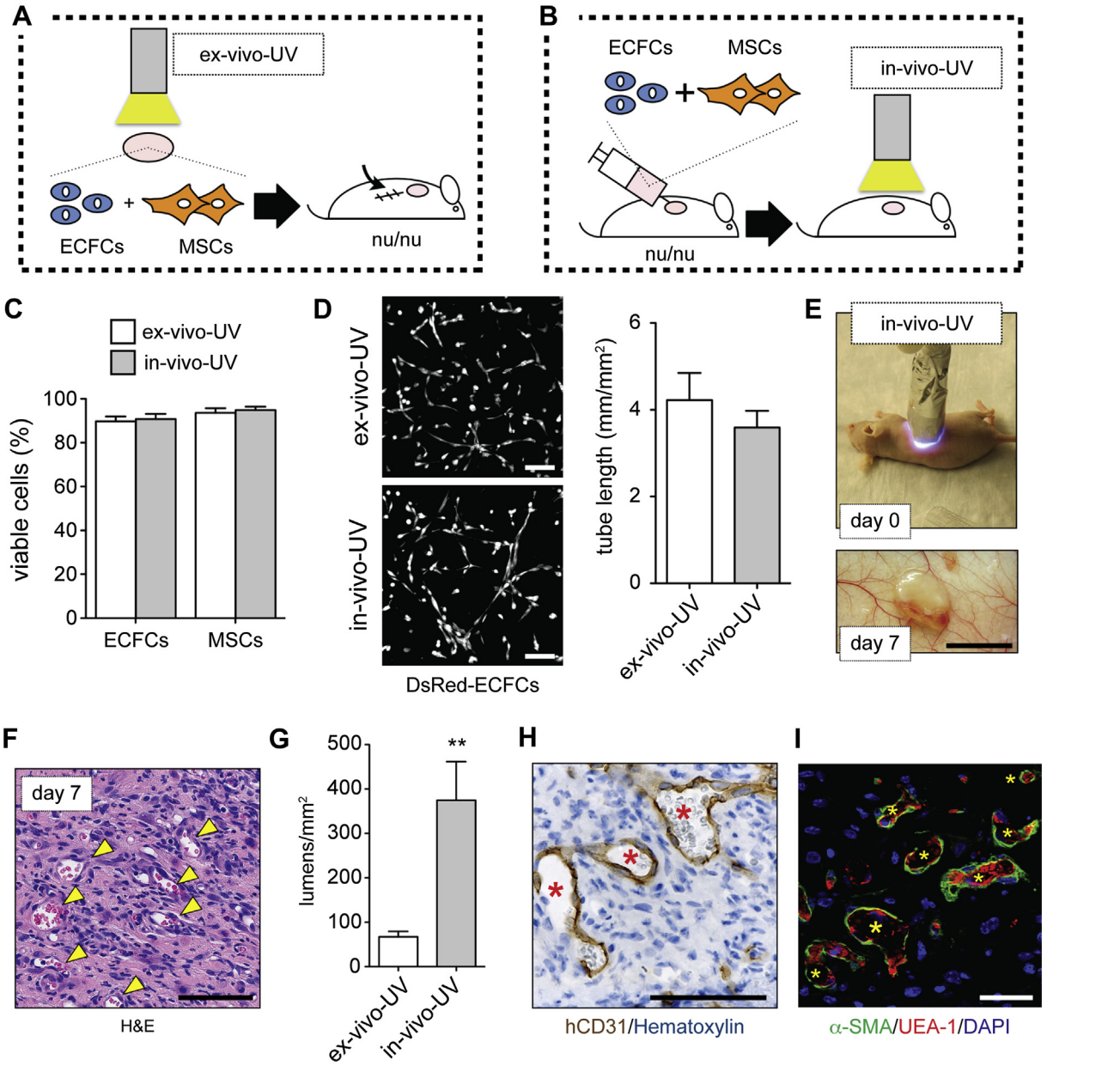

Fig. 2. Transdermal polymerization of GelMA and vascularization. Schematic diagrams representing (A) ex-vivo-UV polymerization of cell-laden GelMA constructs by direct exposure to UV light prior to surgical implantation into nude mice and (B) in-vivo-UV polymerization by transdermal UV exposure following subcutaneous injection of the cell-laden GelMA solution. (C–D) Effect of ex-vivo-UV and in-vivo-UV polymerization on ECFCs and MSCs after 3 h in vivo. (C) Cell viability evaluated at the time of construct explantation ($n = 3$). (D) In vitro tube formation ability evaluated by culturing explanted constructs for 3 days. Representative fluorescent images depicting DsRed-ECFC-lined tubular structures (scale bar 100 μm). The extent of capillary-like formation was quantified in replicate constructs and reported as total length of tubular structures (mm) per unit of section (mm^2) ($n = 3$). (E–I) Formation of human vascular networks was evaluated after 7 days in vivo. (E) Representative images of a mouse receiving transdermal UV light at day 0 and the construct in the subcutaneous space after 7 days (scale bar 1 cm). (F) Representative H&E-stained section from a day 7 construct that was in-vivo-UV polymerized (yellow arrowheads mark perfused blood vessels) (scale bars 50 μm). (G) Microvessel density was determined at day 7 by counting luminal structures containing erythrocytes ($n = 4$). (H–I) Representative micrographs from day 7 constructs that were in-vivo-UV polymerized. (H) Human $hCD31^+$ lumens (red asterisks) were identified by immunohistochemistry (scale bars 50 μm). (I) Perivascular coverage of human $UEA\text{-}1^+$ lumens (yellow asterisks) was assessed by α-SMA staining. Nuclei were stained with DAPI (scale bars 50 μm). The data are presented as the mean ± SD. $^{**}p < 0.01$. (For interpretation of the references to color in this figure legend, the reader is referred to the web version of this article.)

3.3. Transdermal modulation of neovascularization

The degree of GelMA polymerization can be increased by altering the initial exposure time to UV light (Fig. 1), but excessive polymerization may compromise cellular processes. We studied whether variation of the initial exposure time to UV light could be used as a parameter to modulate cell behavior and ultimately, vascularity inside the constructs. First, we analyzed, ex vivo, the range of exposure time to UV light that was compatible with cell viability and found that both ECFCs and MSCs remained viable (>93%) throughout a wide range of exposure time (0–120 s); cell viability was only negatively affected beyond 300 s of UV light exposure (Fig. 4A). We then selected a narrower working range (15–45 s) and confirmed that, in this range, UV exposure did not affect the capacity of ECFCs and MSCs to attach (Fig. 4B) and proliferate (Fig. 4C) in culture. However, the UV exposure time

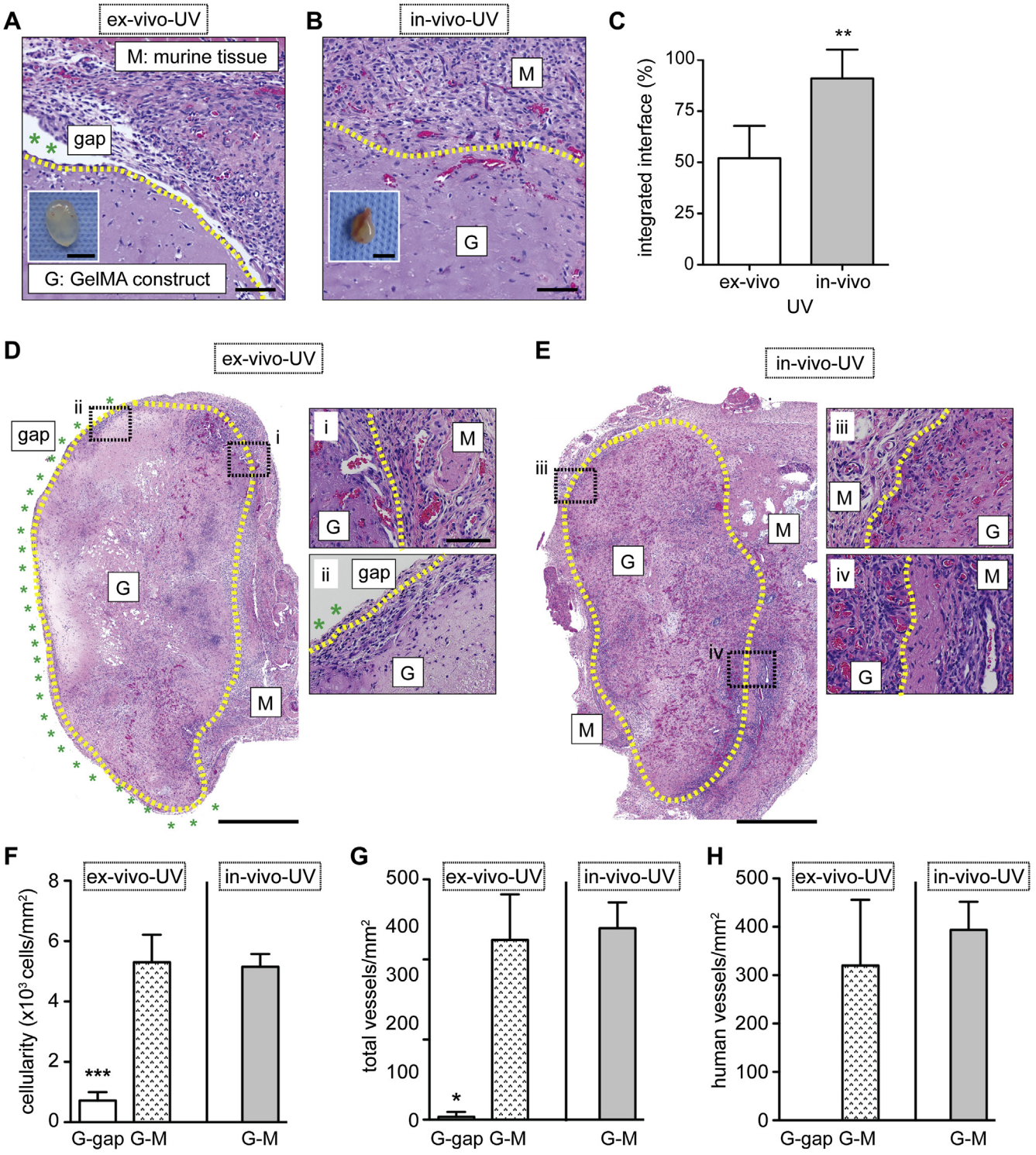

Fig. 3. Regional integration between GelMA and host tissue. Cell-laden GelMA constructs were implanted into nude mice and evaluated after 7 days. (A–B) Representative H&E-stained sections from constructs that were (A) ex-vivo-UV and (B) in-vivo-UV polymerized. Dashed yellow lines mark the boundary between the GelMA constructs [G] and the host murine tissue [M]. Green asterisks mark regions with no integration between construct and host tissue [gap] (scale bars 50 μm). Insets represent macroscopic views of the explants. (C) Intimate contact with the host tissue was quantified as a percentage of total construct perimeter ($n = 4$). (D–E) Representative H&E-stained sections reveal differences in vascularization between regions with full construct-host tissue integration (i, iii, and iv) and regions with no integration (ii) (scale bars 500 μm in complete sections and 50 μm in selected regions). (F) Cellularity, (G) total microvessel density, and (H) human microvessel density at day 7 in regions with full construct-host tissue integration [G-M] and regions with no integration [G-gap] ($n = 4$). The data are presented as the mean ± SD. $^{*}p < 0.05$, $^{**}p < 0.01$, $^{***}p < 0.001$. (For interpretation of the references to color in this figure legend, the reader is referred to the web version of this article.)

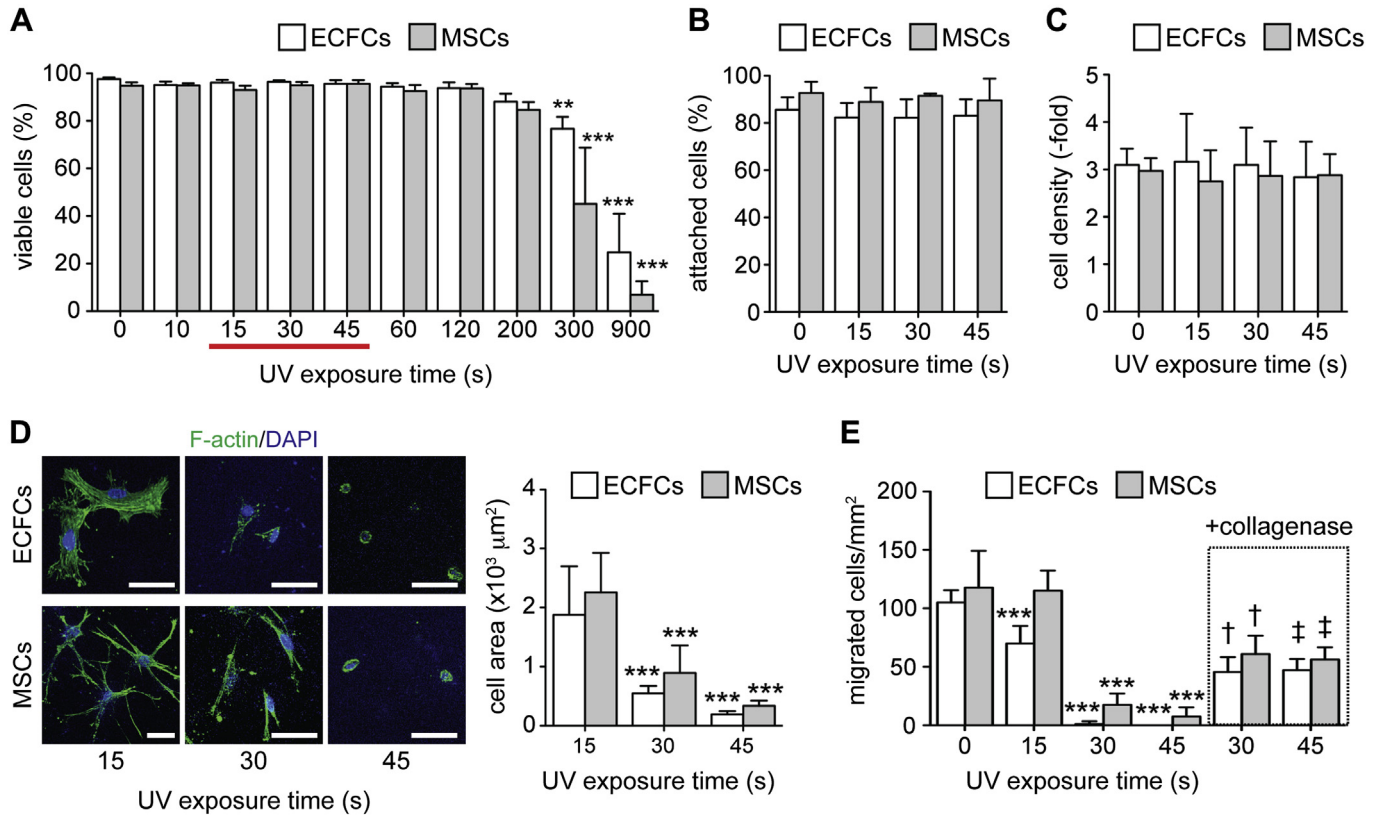

Fig. 4. Effect of UV exposure time on ECFCs and MSCs. (A) Viability, (B) attachment, and (C) proliferation capacity of ECFCs and MSCs after different UV exposure time ($n = 3$). Red line indicates selected working range for UV exposure. (D) Spreading of ECFCs and MSCs embedded in GelMA hydrogels that were polymerized ex vivo using different exposure time to UV light. Images correspond to representative sections of the hydrogels stained with F-actin. Nuclei were stained with DAPI (scale bars 50 μm). Cell spreading was quantified as average cell area ($n = 3$). (E) Migration of ECFCs and MSCs through GelMA polymerized ex vivo using different UV exposure time (0–45 s) ($n = 3$). Migration was also evaluated in the presence of collagenase for GelMA polymerized for 30 s and 45 s ($n = 3$). The data are presented as the mean ± SD. $^{*}p < 0.05$, $^{**}p < 0.01$, $^{***}p < 0.001$ compared to 15 s exposure. †$p < 0.05$, ‡$p < 0.01$ compared to migration in the absence of collagenase. (For interpretation of the references to color in this figure legend, the reader is referred to the web version of this article.)

modulated cell spreading and motility in GelMA hydrogels. Specifically, we found that increasing the UV exposure time from 15 s to 45 s progressively diminished the capacity of both ECFCS and MSCs to spread inside GelMA (Fig. 4D), as well as the ability to migrate through GelMA (Fig. 4E). These results were anticipated because longer exposure to UV light increases the degree of GelMA polymerization; in fact, provision of exogenous collagenase partially recovered the migratory capacity of the cells after prolonged (30–45 s) UV exposure (Fig. 4E), suggesting that cell spreading and motility were likely inhibited as a result of GelMA over-crosslinking (all GelMA hydrogels in the 30–45 s UV exposure range were relatively soft and had similar stiffness; Fig. 1C).

We then examined whether transdermal application of UV light could be used to modulate vascular morphogenesis in vivo (Fig. 5). To this aim, we injected cell-laden GelMA into nude mice and applied UV light for either 15 s, 30 s, or 45 s (Fig. 5). After 7 days, the GelMA constructs were explanted and examined for the presence of vascular structures. H&E staining revealed that the extent of vascular network formation was indeed affected by the initial UV exposure time (Fig. 5A). Quantitative evaluation of the explants revealed a progressive reduction in the total number of perfused blood vessels as the original UV exposure time was increased from 15 s (374.7 ± 174.2 lumens/mm^2) to 30 s (145.1 ± 105.5 lumens/mm^2); no blood vessels were detected inside the constructs that were exposed for 45 s (Fig. 5D). In addition, the initial UV exposure time affected the morphology of the newly formed human microvessels, which were identified as hCD31$^+$ (Fig. 5B) and UEA-1$^+$ (Fig. 5C) lumens. Specifically, lumens in constructs that were photocrosslinked for 15 s were significantly larger (96.12 ± 10.5 μm^2) than those in constructs that were photocrosslinked for 30 s (39.1 ± 5.3 μm^2) (Fig. 5 E). In the former group (15 s), most human microvessels had distinguishable lumens (Fig. 5B, C). However, in the 30 s group, the presence of well-formed lumens alternated with non-lumenal ECFC-lined cord structures (Fig. 5B, C) and eventual non-assembled individual ECFCs. Finally, in the 45 s group, hCD31$^+$/UEA-1$^+$ ECFCs were predominantly found as individual cells, suggesting a lack of cellular motility. Collectively, these results demonstrated that both the overall vascular density and the average lumen size can be modulated by changing, transdermally, the initial exposure time to UV light.

3.4. Interaction between GelMA hydrogel and host cells

We previously demonstrated that recruitment of host myeloid cells is a necessary step in ECFC/MSC-mediated neovascularization [25]. Here we examined whether the differences observed in microvascular density between constructs exposed to UV light for 15 s and 30 s were associated with a differential recruitment of host cells (Fig. 6). To this aim, we examined constructs from both groups after 2 days in vivo. H&E-stained sections revealed that in the boundaries between constructs (G) and host tissue (M) cellularity was significantly higher in the 15 s group than in the 30 s one (Fig. 6A), suggesting differential infiltration of host cells. We then quantified the presence of murine myeloid cells (mCD45$^+$/mCD11b$^+$) and ECs (mCD45$^-$/mCD31$^+$) by flow cytometry in cells that were retrieved from

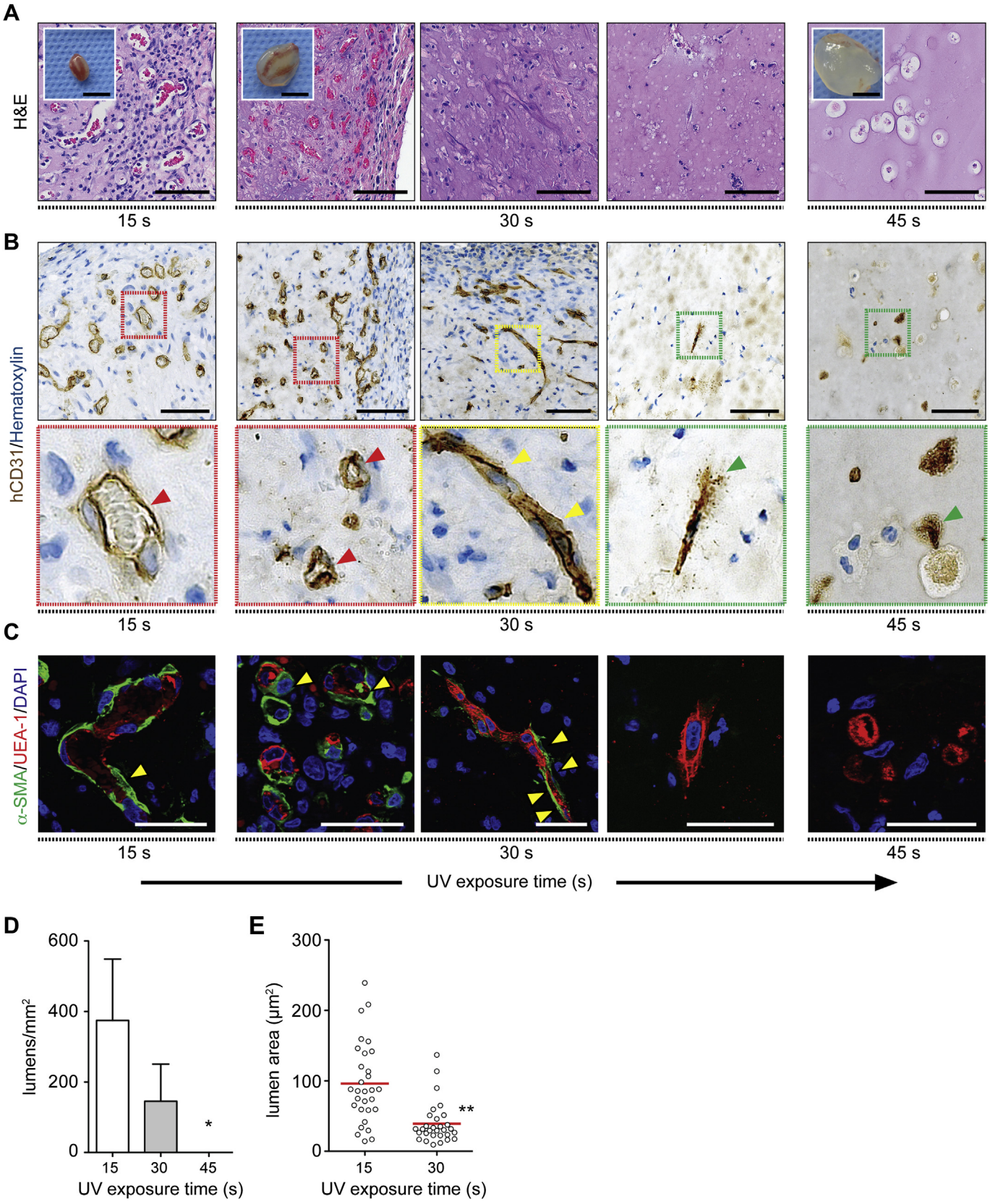

Fig. 5. Transdermal modulation of vascular network bioengineering. Cell/GelMA solutions were subcutaneously injected into nude mice and polymerized by transdermal exposure to UV light. Constructs were evaluated after 7 days in vivo. (A) Representative H&E-stained sections from constructs that were initially exposed to UV light for 15, 30, and 45 s (scale bars 50 μm). Insets represent macroscopic views of the explants (scale bars 5 mm). (B) Human hCD31$^+$ ECFCs were identified by immunohistochemistry (scale bars 50 μm in top panels). Red-lined regions represent areas with perfused lumens lined by hCD31$^+$ ECFCs. The yellow-lined region represents an area with CD31$^+$ ECFCs forming a non-lumenal cord-like structure. Green-lined regions represent areas with individual hCD31$^+$ ECFCs. High magnification of selected regions is depicted in bottom panels, with red, yellow, and green arrowheads pointing

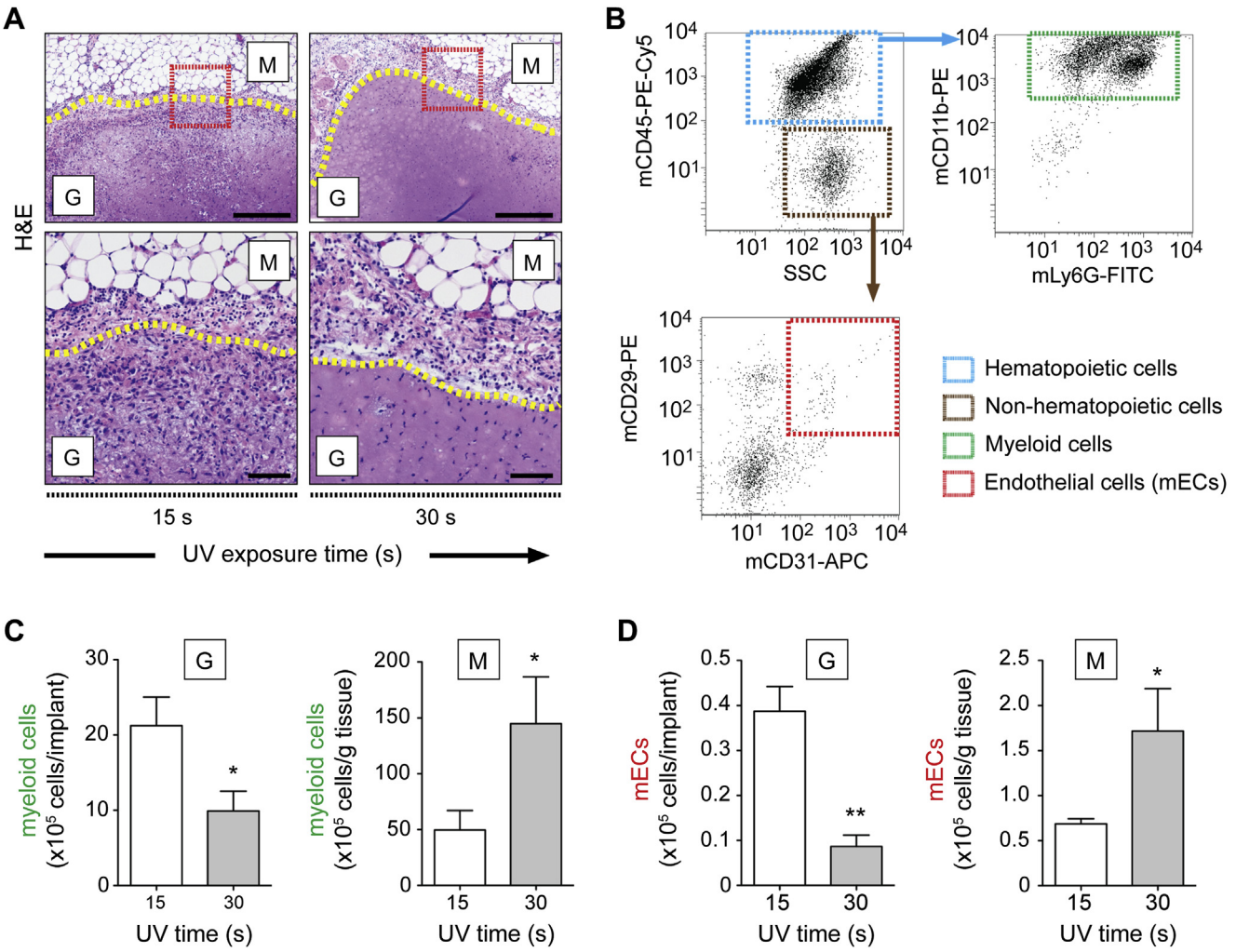

Fig. 6. Modulation of host cell recruitment. Cell/GelMA solutions were subcutaneously injected into nude mice and polymerized by transdermal exposure to UV light for either 15 s or 30 s. Constructs were evaluated after 2 days in vivo. (A) Representative H&E-stained sections of the constructs (scale bars 200 μm in top panels). Dashed yellow lines mark the boundary between the GelMA constructs [G] and the host murine tissue [M]. High magnifications of selected regions are depicted in the bottom panels (scale bars 50 μm). (B–D) Flow cytometry analysis of cells that were retrieved from the constructs at day 2 by enzymatic digestion. (B) Representative flow cytometry panels and regions for identification of murine myeloid ($mCD45^+/mCD11b^+$) and endothelial ($mCD45^-/mCD29^+/mCD31^+$) cells. (C) Quantification of total murine myeloid cells and (D) murine endothelial cells in both the GelMA constructs [G] and the surrounding host tissue [M]. The data are presented as the mean ± SD ($n = 4$). $^*p < 0.05$, $^{**}p < 0.01$ compared to 15 s UV exposure. (For interpretation of the references to color in this figure legend, the reader is referred to the web version of this article.)

explanted constructs (G) and the surrounding host tissue (M) (Fig. 6B–D). We found that the number of host myeloid cells (Fig. 6C) and ECs (Fig. 6D) that had infiltrated the constructs was significantly higher in the 15 s group than in the 30 s one. Moreover, lower infiltration of host cells was associated with higher presence in the surrounding host tissue, suggesting that the infiltration process itself was partially impaired in the 30 s group. Taken together, these results indicated that the interaction of host cells with the constructs was modulated by changing the degree of GelMA polymerization.

3.5. Comparison with other natural hydrogels

We compared the extent of vascular network formation in GelMA constructs to other injectable hydrogels commonly used in this field of research, namely Matrigel and bovine type-I collagen (Fig. 7). As expected from our own previous studies, both Matrigel and type-I collagen were suitable for ECFC/MSC-mediated vascular network formation [4]. However, quantitative analysis of H&E-stained sections taken from explanted constructs at day 7 revealed that the extent of vascular network formation was significantly higher in GelMA (374.7 ± 174.2 lumens/mm^2) than in collagen (185.7 ± 47.0 lumens/mm^2) and Matrigel (103.3 ± 40.1 lumens/mm^2) (Fig. 5C). The human specificity of these microvessels was confirmed by immunohistochemistry ($hCD31^+$ lumens in Fig. 7B).

4. Discussion

Hydrogels can be formulated to have structural similarities with soft human tissues and are widely used as materials in biomedical applications [16,26]. There are several hydrogel formulations that

at $hCD31^+$ lumens, $hCD31^+$ cords, and individual $hCD31^+$ ECFCs, respectively. (C) Perivascular coverage of human UEA-1^+ lumens (yellow arrowheads) was assessed by α-SMA staining. Nuclei were stained with DAPI (scale bars 50 μm). (D) Microvessel density was determined at day 7 by counting luminal structures containing erythrocytes ($n = 4$). (E) Microvascular lumen area was quantified in constructs that were initially exposed to UV light for 15 s and 30 s ($n = 4$). The data are presented as the mean ± SD. $^*p < 0.05$, $^{**}p < 0.01$ compared to 15 s UV exposure. (For interpretation of the references to color in this figure legend, the reader is referred to the web version of this article.)

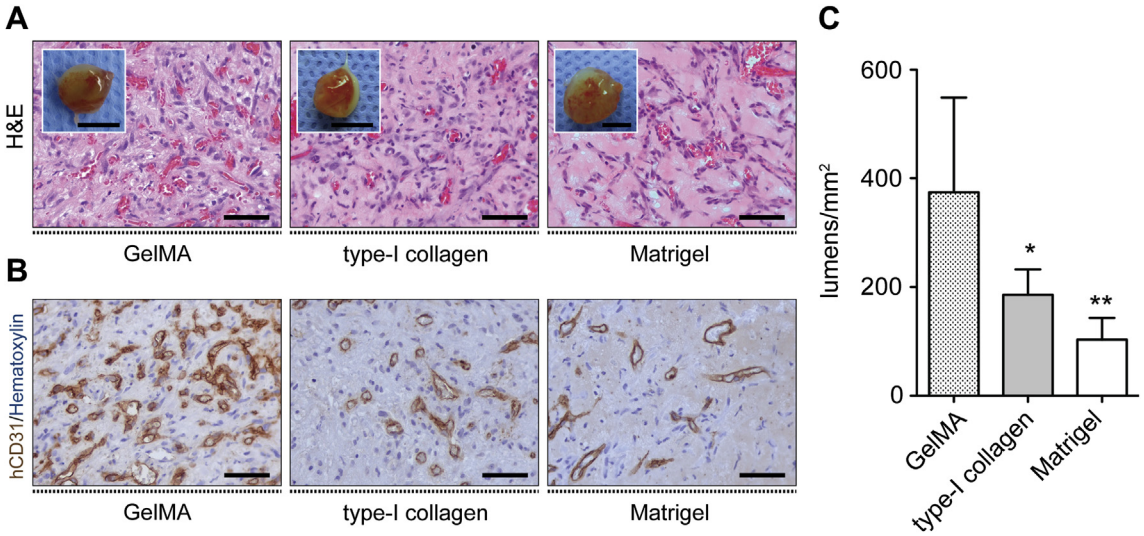

Fig. 7. Comparative evaluation of GelMA, Matrigel, and type-I collagen hydrogels. Human ECFCs and MSCs (total 2×10^6 cells; 2:3 ECFC:MSC ratio) were resuspended in a solution of either GelMA, type-I collagen, or Matrigel and subcutaneously injected into nude mice (final volume: 200 μL). GelMA implants were polymerized by transdermal exposure to UV light for 15 s. Constructs were evaluated after 7 days in vivo. (A) Representative H&E-stained sections from each hydrogel group with visible presence of erythrocyte-filled microvessels (scale bars 50 μm). Insets represent macroscopic views of the explants (scale bars 5 mm). (B) Human $hCD31^+$ lumens were identified by immunohistochemistry in each hydrogel group (scale bars 50 μm). (C) Microvessel density was determined at day 7 by counting luminal structures containing erythrocytes. The data are presented as the mean ± SD ($n = 4$). $^*p < 0.05$, $^{**}p < 0.01$ compared to GelMA.

are synthesized from natural biopolymers such as collagen and fibrin that can successfully recapitulate suitable environments for vascular morphogenesis and are commonly proposed as cellular scaffolds for vascular network bioengineering [7,27–31]. Nevertheless, in certain tissue engineering applications, the inherent advantages of most natural hydrogels (namely, soft conformation, biodegradability) may become disadvantageous (e.g., insufficient mechanical strength, low durability), which drives the continuous search for alternative formulations [32]. Numerous alternative biomaterials have been proposed for specific biomedical applications over the past decade, including hydrogels made from both synthetic (e.g., poly(vinyl alcohol), poly(ethylene oxide), poly(-acrylic acid)) and naturally occurring (e.g., hyaluronate, alginate, agarose, chitosan and its derivatives) polymers [33]. One such alternative is GelMA, a hydrogel that is synthesized by adding methacrylate groups to the amine-containing side-groups of gelatin, becoming a photocrosslinkable material in the presence of a photoinitiator [17]. GelMA hydrogel has several advantages due to its dual natural and synthetic properties. For instance, GelMA contains gelatin as its backbone, which provides cell-responsive characteristics including the provision of appropriate cell adhesion sites and proteolytic degradability [17,33]. Meanwhile, the ability to modulate the degree of methacrylation enables tuning the final mechanical and chemical properties of the hydrogel [17,18]. In a previous study, we demonstrated that GelMA can be formulated to support human vascular morphogenesis [18]. We showed that ECFCs/MSCs embedded in GelMA can form extensive vascular networks that connect with the host vasculature after implantation into mice. This initial proof-of-concept study was carried out by first polymerizing the cell-laden GelMA constructs ex vivo, followed by a period of tissue culture prior to surgical implantation into the subcutaneous space of nude mice. However, the full clinical potential of GelMA will be best harnessed by enabling in situ polymerization [34]. In this manner, liquid GelMA could flow through small-bore needles or catheters prior to its final polymerized conformation, facilitating minimally invasive implantation. In this study, we demonstrated the feasibility of bioengineering functional human vascular networks inside GelMA constructs that were first subcutaneously injected into immunodeficient mice while in liquid form, and then transdermally photopolymerized using UV light.

Photopolymerization via direct exposure of materials to light is commonly used in medicine in open environments such as the oral cavity or during certain surgical procedures [35–38]. In addition, studies have demonstrated that UV and visible light can penetrate the skin and polymerize photocrosslinkable materials in situ [21,39]. However, combining transdermal photopolymerization with cell delivery presents additional challenges, including preserving the viability and functionality of the cells [40]. Injecting GelMA in its liquid form should be followed by rapid polymerization in order to avoid hydrogel leakage into the neighboring tissues and excessive dilution with body fluids, both of which can compromise cellular confinement and the final conformation of the construct. We formulated GelMA so that transdermal polymerization occurred after a few seconds of UV exposure (15 s was sufficient to fully crosslink a 200 μL construct). Injecting GelMA eliminated the need for both pre-polymerizing the constructs and surgical incisions. Most notably, we found that injecting GelMA in its liquid form conferred additional advantages, including improved integration between the hydrogel constructs and the surrounding host tissue. The result was better vascularity (~3-fold) in injected constructs than in constructs that were polymerized ex vivo prior to implantation.

Transdermal exposure to our UV light spectrum (UVA-visible: 320–500 nm) had little observable effect on the human cells themselves; both ECFCs and MSCs remained completely viable and functional after prolonged (up to 120 s) exposure to UV light. However, GelMA properties (mainly, its degree of polymerization) are sensitive to changes in UV exposure time [17]. Thus, we expected vascular morphogenesis, which is an orchestrated process between the cells and their surrounding ECM environment, to be affected by the UV exposure time. On the one hand, we found that GelMA constructs that were photocrosslinked for 15 s formed an extensive network of ECFC-lined microvessels after 7 days in vivo; these microvessels had well-formed lumens that were filled with murine erythrocytes and were uniformly distributed throughout

the constructs. On the other hand, constructs that were photocrosslinked for 45 s did not form lumenal structures and ECFCs were predominantly distributed as individual cells. This lack of ECFC assembly was not attributed to the cells themselves, which were viable and functional. Instead, the lack of vascularization was directly attributed to excessive GelMA crosslinking, which impaired cell (both donor and host) motility throughout the construct. In fact, constructs with an intermediate degree of polymerization (30 s UV exposure) presented intermediate vascular features, including well-formed ECFC-lined lumenal structures, cord-like (but non-lumenal) structures, and individual non-associated ECFCs. In addition, the average size of the bioengineered lumens was significantly larger in constructs that were less polymerized, indicating that the degree of photocrosslinking had a direct influence not only on vascular uniformity and density, but it also modulated the actual luminal size of the vessels. Moreover, the interaction of host cells with the constructs was also altered by the degree of polymerization, with significantly less penetration (but more accumulation in the boundary) of both murine myeloid and ECs in constructs that were crosslinked for a longer period of time. This is important because accessibility of host cells is critical for ECFC-mediated vasculogenesis [25], sprouting of host microvessels via angiogenesis [41–43], and ultimately formation of anastomosis between bioengineered vessels and host sprouts [44].

Collectively, our results have two main implications. First, we have demonstrated that vascularization can be directly modulated by adjusting transdermal exposure time to UV light. This capacity to modulate vascular density could be instrumental to differentially bioengineer tissues that have, in principle, different vascular requirements [45]. Second, our results illustrate that formulating a suitable hydrogel can be complex and it requires not only accounting for biocompatibility and biodegradability, but also understanding the specific nature of the cells under consideration as well as the biological processes that we expect these cells to carry out. In our case, even though GelMA could in practice be polymerized to obtain a wide range of mechanical properties, only few GelMA conformations (those obtained after 15–30 s exposure to UV light) were found to be compatible with sufficient ECFC/MSC motility and spreading, recruitment of host cells, and ultimately vascular morphogenesis. Nevertheless, we found robust formation of human microvessels within this range of GelMA polymerization. To put our results in perspective, our cell-laden GelMA constructs (15 s) had significant higher vascular densities than those constructs made with the same exact cells using other common hydrogels (namely, Matrigel or type-I collagen). Numerous studies have shown that several natural hydrogels can recapitulate permissive environments for vascular morphogenesis [7,27–31]. However, it is the capacity to modulate vascularization that makes GelMA an advantageous hydrogel material for applications that require the formation of functional vascular beds, including the engineering of complex tissues.

5. Conclusions

In the present study, we have demonstrated the suitability of a photocrosslinkable GelMA hydrogel to undergo transdermal polymerization while supporting human progenitor cell-based formation of vascular networks in vivo. Specifically, we have shown that a liquid solution of GelMA containing human blood-derived ECFCs and bone marrow-derived MSCs can be injected into the subcutaneous space of an immunodeficient mouse and then rapidly crosslinked (15–30 s) by transdermal exposure to UV light, forming a three-dimensional cell-laden polymerized construct. After polymerization, the implanted human cells generated an extensive vascular network that formed functional anastomoses with the host vasculature and was uniformly distributed throughout the construct. We have also demonstrated that the degree of GelMA polymerization is controllable through the exposure time to UV light and that this capacity to modulate the mechanical properties of the hydrogel can be used to tune vascular morphogenesis and ultimately the extent of vascular network formation inside each construct. Based on these data, we propose the use of GelMA in its injectable form, followed by in situ photopolymerization, as a means to deliver vascular cells in future regenerative applications that require the formation of functional vascular beds in vivo.

Acknowledgments

This work was supported by National Institutes of Health grants (R00EB009096, to J.M.M.-M; R01HL092836, R01HL099073, and AR057837, to A.K.) and a National Science Council of Republic of China grant (NSC101-2221-E-134-001, to Y.-C.C).

Appendix A. Supplementary material

Supplementary data related to this article can be found online at http://dx.doi.org/10.1016/j.biomaterials.2013.05.060.

References

[1] Lin Y, Weisdorf DJ, Solovey A, Hebbel RP. Origins of circulating endothelial cells and endothelial outgrowth from blood. J Clin Invest 2000;105:71–7.
[2] Ingram DA, Mead LE, Tanaka H, Meade V, Fenoglio A, Mortell K, et al. Identification of a novel hierarchy of endothelial progenitor cells using human peripheral and umbilical cord blood. Blood 2004;104:2752–60.
[3] Ingram DA, Mead LE, Moore DB, Woodard W, Fenoglio A, Yoder MC. Vessel wall-derived endothelial cells rapidly proliferate because they contain a complete hierarchy of endothelial progenitor cells. Blood 2005;105:2783–6.
[4] Melero-Martin J, De Obaldia ME, Kang S-Y, Khan ZA, Yuan L, Oettgen P, et al. Engineering robust and functional vascular networks in vivo with human adult and cord blood-derived progenitor cells. Circ Res 2008;103:194–202.
[5] Au P, Daheron LM, Duda DG, Cohen KS, Tyrrell JA, Lanning RM, et al. Differential in vivo potential of endothelial progenitor cells from human umbilical cord blood and adult peripheral blood to form functional long-lasting vessels. Blood 2007;111:1302–5.
[6] Traktuev DO, Prater DN, Merfeld-Clauss S, Sanjeevaiah AR, Saadatzadeh MR, Murphy M, et al. Robust functional vascular network formation in vivo by cooperation of adipose progenitor and endothelial cells. Circ Res 2009;104:1410–20.
[7] Chen X, Aledia AS, Popson SA, Him L, Hughes CCW, George SC. Rapid anastomosis of endothelial progenitor cell-derived vessels with host vasculature is promoted by a high density of cotransplanted fibroblasts. Tissue Eng Part A 2010;16:585–94.
[8] Melero-Martin J, Khan ZA, Picard A, Wu X, Paruchuri S, Bischoff J. In vivo vasculogenic potential of human blood-derived endothelial progenitor cells. Blood 2007;109:4761–8.
[9] Yoder MC, Mead LE, Prater D, Krier TR, Mroueh KN, Li F, et al. Redefining endothelial progenitor cells via clonal analysis and hematopoietic stem/progenitor cell principals. Blood 2007;109:1801–9.
[10] Lin R-Z, Dreyzin A, Aamodt K, Li D, Jaminet S-CS, Dudley AC, et al. Induction of erythropoiesis using human vascular networks genetically engineered for controlled erythropoietin release. Blood 2011;118:5420–8.
[11] Allen P, Melero-Martin J, Bischoff J. Type I collagen, fibrin and PuraMatrix matrices provide permissive environments for human endothelial and mesenchymal progenitor cells to form neovascular networks. J Tissue Eng Regen Med 2011;5:e74–86.
[12] Kleinman HK, Martin GR. Matrigel: basement membrane matrix with biological activity. Semin Cancer Biol 2005;15:378–86.
[13] Janmey PA, Winer JP, Weisel JW. Fibrin gels and their clinical and bioengineering applications. J R Soc Interface 2009;6:1–10.
[14] Helary C, Bataille I, Abed A, Illoul C, Anglo A, Louedec L, et al. Concentrated collagen hydrogels as dermal substitutes. Biomaterials 2010;31:481–90.
[15] Hanjaya-Putra D, Bose V, Shen Y, Yee J. Controlled activation of morphogenesis to generate a functional human microvasculature in a synthetic matrix. Blood 2011;118:804–15.
[16] Slaughter BV, Khurshid SS, Fisher OZ, Khademhosseini A, Peppas NA. Hydrogels in regenerative medicine. Adv Mater 2009;21:3307–29.
[17] Nichol JW, Koshy ST, Bae H, Hwang CM, Yamanlar S, Khademhosseini A. Cell-laden microengineered gelatin methacrylate hydrogels. Biomaterials 2010;31:5536–44.
[18] Chen Y-C, Lin R-Z, Qi H, Yang Y, Bae H, Melero-Martin J, et al. Functional human vascular network generated in photocrosslinkable gelatin methacrylate hydrogels. Adv Funct Mater 2012;22:2027–39.

[19] Nikkhah M, Eshak N, Zorlutuna P, Annabi N, Castello M, Kim K, et al. Directed endothelial cell morphogenesis in micropatterned gelatin methacrylate hydrogels. Biomaterials 2012;33:9009–18.
[20] Ramón-Azcón J, Ahadian S, Obregón R, Camci-Unal G, Ostrovidov S, Hosseini V, et al. Gelatin methacrylate as a promising hydrogel for 3D microscale organization and proliferation of dielectrophoretically patterned cells. Lab Chip 2012;12:2959–69.
[21] Elisseeff J, Anseth K, Sims D, McIntosh W, Randolph M, Langer RS. Transdermal photopolymerization for minimally invasive implantation. Proc Natl Acad Sci U S A 1999;96:3104–7.
[22] Van Den Bulcke AI, Bogdanov B, De Rooze N, Schacht EH, Cornelissen M, Berghmans H. Structural and rheological properties of methacrylamide modified gelatin hydrogels. Biomacromolecules 2000;1:31–8.
[23] Lin R-Z, Moreno-Luna R, Zhou B, Pu WT, Melero-Martin J. Equal modulation of endothelial cell function by four distinct tissue-specific mesenchymal stem cells. Angiogenesis 2012;15:443–55.
[24] International Agency for Research on Cancer (IARC). Exposure to artificial UV radiation and skin cancer. IARC working group reports No 1. IARC; 2006.
[25] Melero-Martin J, De Obaldia ME, Allen P, Dudley AC, Klagsbrun M, Bischoff J. Host myeloid cells are necessary for creating bioengineered human vascular networks in vivo. Tissue Eng Part A 2010;16:2457–66.
[26] Peppas NA, Hilt JZ, Khademhosseini A, Langer RS. Hydrogels in biology and medicine: from molecular principles to bionanotechnology. Adv Mater 2006;18:1345–60.
[27] Schechner JS, Nath AK, Zheng L, Kluger MS, Hughes CCW, Sierra-Honigmann MR, et al. In vivo formation of complex microvessels lined by human endothelial cells in an immunodeficient mouse. Proc Natl Acad Sci U S A 2000;97:9191–6.
[28] Koike N, Fukumura D, Gralla O, Au P, Schechner JS, Jain RK. Tissue engineering: creation of long-lasting blood vessels. Nature 2004;428:138–9.
[29] Stratman AN, Saunders WB, Sacharidou A, Koh W, Fisher KE, Zawieja DC, et al. Endothelial cell lumen and vascular guidance tunnel formation requires MT1-MMP-dependent proteolysis in 3-dimensional collagen matrices. Blood 2009;114:237–47.
[30] Jay SM, Shepherd BR, Andrejecsk JW, Kyriakides TR, Pober JS, Saltzman WM. Dual delivery of VEGF and MCP-1 to support endothelial cell transplantation for therapeutic vascularization. Biomaterials 2010;31:3054–62.
[31] Ehrbar M, Djonov VG, Schnell C, Tschanz SA, Martiny-Baron G, Schenk U, et al. Cell-demanded liberation of VEGF121 from fibrin implants induces local and controlled blood vessel growth. Circ Res 2004;94:1124–32.
[32] Anderson DG, Burdick JA, Langer RS. Materials science. Smart biomaterials. Science 2004;305:1923–4.
[33] Lee KY, Mooney DJ. Hydrogels for tissue engineering. Chem Rev 2001;101:1869–79.
[34] Bencherif SA, Sands RW, Bhatta D, Aranya P, Verbeke CS, Edwards DA, et al. Injectable preformed scaffolds with shape-memory properties. Proc Natl Acad Sci U S A 2012;109:19590–5.
[35] Venhoven BAM, de Gee AJ, Davidson CL. Polymerization contraction and conversion of light-curing BisGMA-based methacrylate resins. Biomaterials 1993;14:871–5.
[36] Hill-West JL, Chowdhury SM, Slepian MJ, Hubbell JA. Inhibition of thrombosis and intimal thickening by in situ photopolymerization of thin hydrogel barriers. Proc Natl Acad Sci U S A 1994;91:5967–71.
[37] Mehl A, Hickel R, Kunzelmann KH. Physical properties and gap formation of light-cured composites with and without 'softstart-polymerization'. J Dent 1997;25:321–30.
[38] Davidson CL, de Gee AJ. Light-curing units, polymerization, and clinical implications. J Adhes Dent 2000;2:167–73.
[39] Hillel AT, Unterman S, Nahas Z, Reid B, Coburn JM, Axelman J, et al. Photoactivated composite biomaterial for soft tissue restoration in rodents and in humans. Sci Transl Med 2011;3:93ra67.
[40] Nguyen KT, West JL. Photopolymerizable hydrogels for tissue engineering applications. Biomaterials 2002;23:4307–14.
[41] Roh JD, Sawh-Martinez R, Brennan MP, Jay SM, Devine L, Rao DA, et al. Tissue-engineered vascular grafts transform into mature blood vessels via an inflammation-mediated process of vascular remodeling. Proc Natl Acad Sci U S A 2010;107:4669–74.
[42] Anghelina M, Krishnan P, Moldovan L, Moldovan NI. Monocytes/macrophages cooperate with progenitor cells during neovascularization and tissue repair: conversion of cell columns into fibrovascular bundles. Am J Pathol 2006;168:529–41.
[43] Tigges U, Hyer EG, Scharf J, Stallcup WB. FGF2-dependent neovascularization of subcutaneous matrigel plugs is initiated by bone marrow-derived pericytes and macrophages. Development 2008;135:523–32.
[44] Fantin A, Vieira J, Gestri G, Denti L, Schwarz Q. Tissue macrophages act as cellular chaperones for vascular anastomosis downstream of VEGF-mediated endothelial tip cell induction. Blood 2010;116:829–40.
[45] Mammoto A, Connor KM, Mammoto T, Yung CW, Huh D, Aderman CM, et al. A mechanosensitive transcriptional mechanism that controls angiogenesis. Nature 2009;457:1103–8.